10TH ADVANCED TRAINING COURSE ON LAND REMOTE SENSING

Natural disturbances of forests : lecture

Oleg Antropov, VTT Technical Research Centre of Finland

Overview

- Introduction
- SAR imaging sensors, data and processing
- Change detection approaches
- Demonstration use-cases
    - mapping snow damaged forest using Sentinel-1 image time series
    - mapping wind-thrown forest using Sentinel-1 image time series and auxiliary data
    - Autochange in forest disturbance mapping using Sentinel-2 imagery
- Practical session: SNAP graph-based processing, stand-level feature calculation and SVM classification using Python libraries.

Types of forest disturbances

- Anthropogenic disturbances
  - Forest management operations
  - Slash and burn agriculture
  - Small-scale collection of brunches
  - Land cover/use type conversion
- Natural forest disturbances
  - Forest fires (mapping of burned areas and active fire detection)
  - Forest windthrows
  - Insect damage
  - Snow-damage

Further, we discuss primarily SAR and SAR+optical data based approaches in forest disturbance mapping

SAR image analysis as an inverse problem

$$I(x,y) = F[\ldots, \{\text{ target properties }\}, \ldots]$$

{ target properties} :
{moisture,
roughness,
orientation,
vertical structure,
density,
spatial structure}

$$\{\text{ target properties }\} = F^{-1}[\, I(x,y)\,]$$

Basic exploitation of SAR images: backscattering coefficient

- Values of σ_0 are directly related to the scene properties
  - Strong influence of acquisition geometry and frequency band on the response from targets
  - Many different causes may produce the same σ_0 value: e.g. soil moisture, ground roughness, presence of small plants, etc.
- Biophysical parameter retrieval:
  - by inverting forward scattering models
  - statistical (empirical, semi-empirical) relationship can be established between SAR observables and biophysical

… many parameters for a single observable

Different sensitivity to geometrical and electrophysical properties of illuminated targets

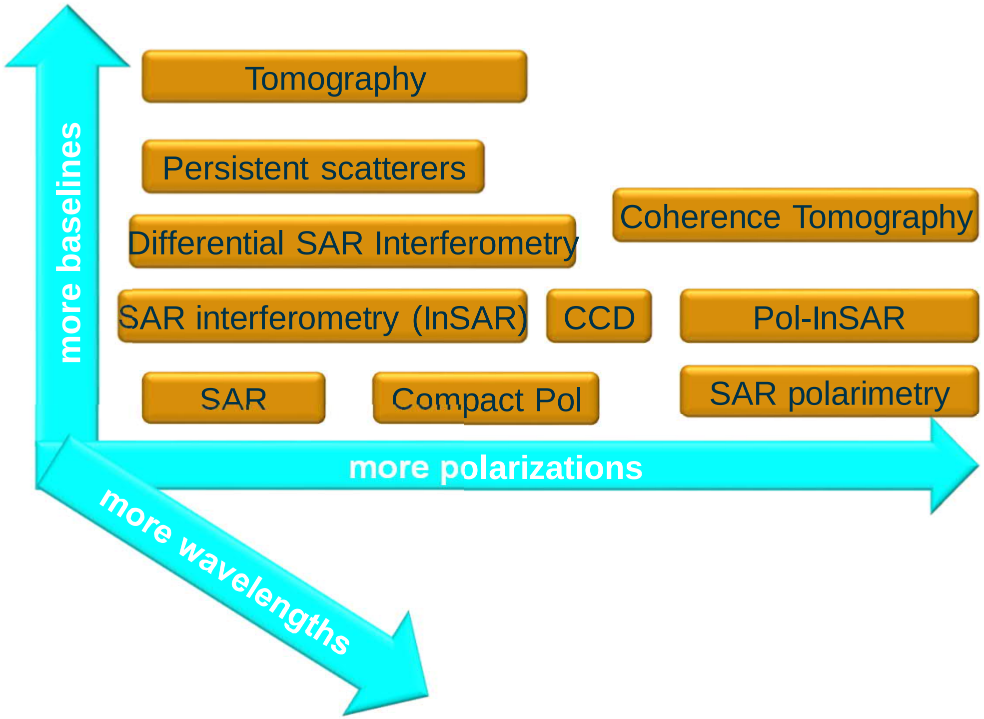

Increasing parameter-space:

- Multitemporal
- Multifrequency
- Multi-sensor
- Multi angular
- Interferometric
- Multibaseline
- Multi-polarization
- Various combinations

Recent SAR sensors

- Sentinel-1A,B
- RADARSAT-2
- ALOS-2 PALSAR-2
- TerraSAR-X TanDEM-X
- Cosmo-SkyMed
- ICEYE
- Capella Space

Approaching:

- BIOMASS
- Rose-L
- TanDEM-L
- NiSAR

©JAXA, L-band, 2006-2011

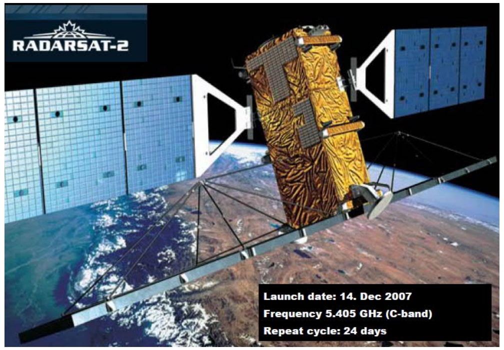

©CSA/MDA, C-band, 2007-now

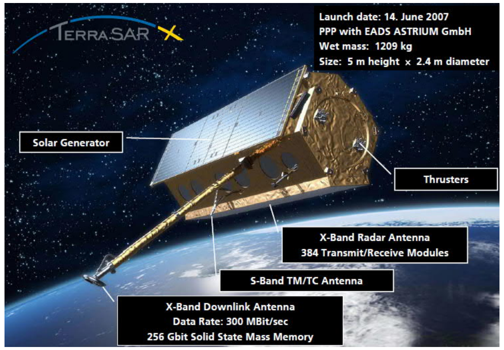

©DLR, X-band, 2007-now

©ASI, X-band, 4, 2007…2010-now

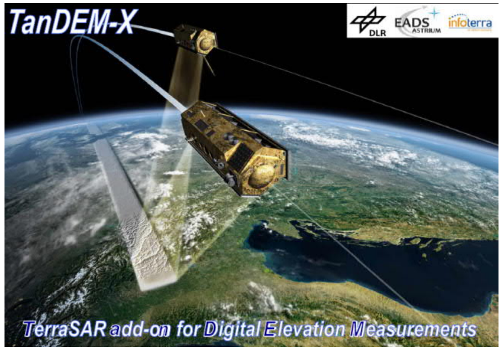

©DLR, X-band, 2010-now

Forest mapping with SAR

- SAR to forest biomass relationship

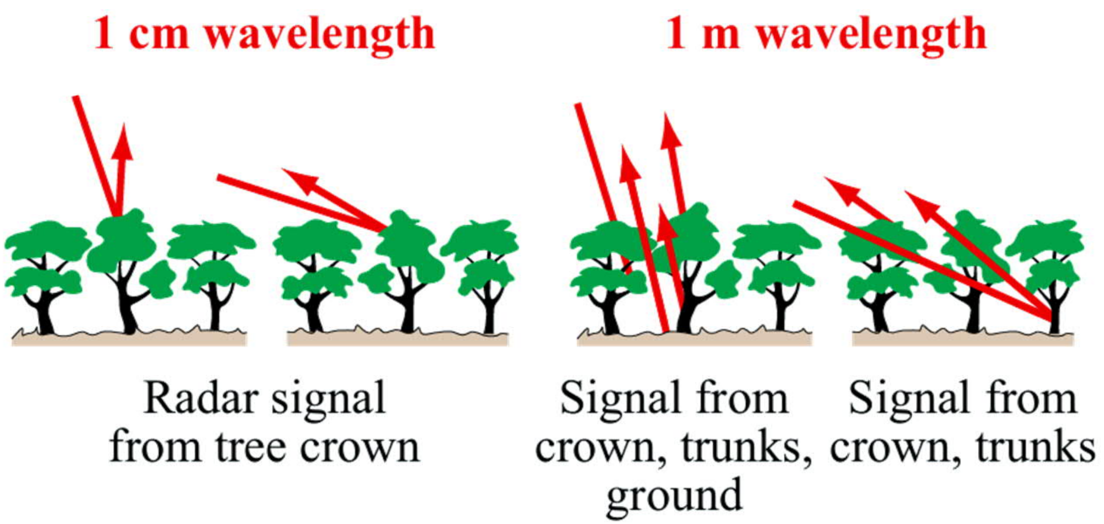

Ulaby and Long. Microwave Radar and Radiometric Remote Sensing, Artech House 2014

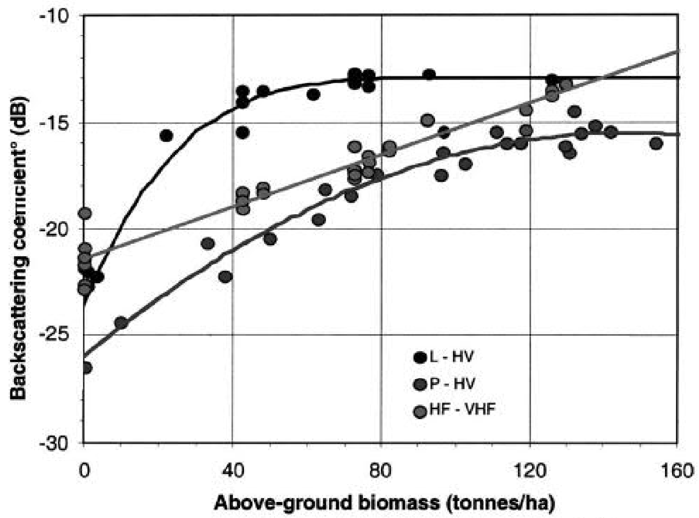

Figure 1. Relationships between the radar backscattering coefficient (in dB m^2/m^2) and above-ground biomass (in tonnes/ha) observed at the Landes forest. The radar measurements are at L-band (wavelength 25 cm) HV polarisation, P band (wavelength 70 cm) HV polarisation, and VHF band (wavelength 3–15 m), HH polarisation.

Le Toan et al., Relating radar remote sensing of biomass to modelling of forest carbon budgets, J. of Climatic Change, 2004.

- SAR to forest biomass relationship (boreal forest at L-band)

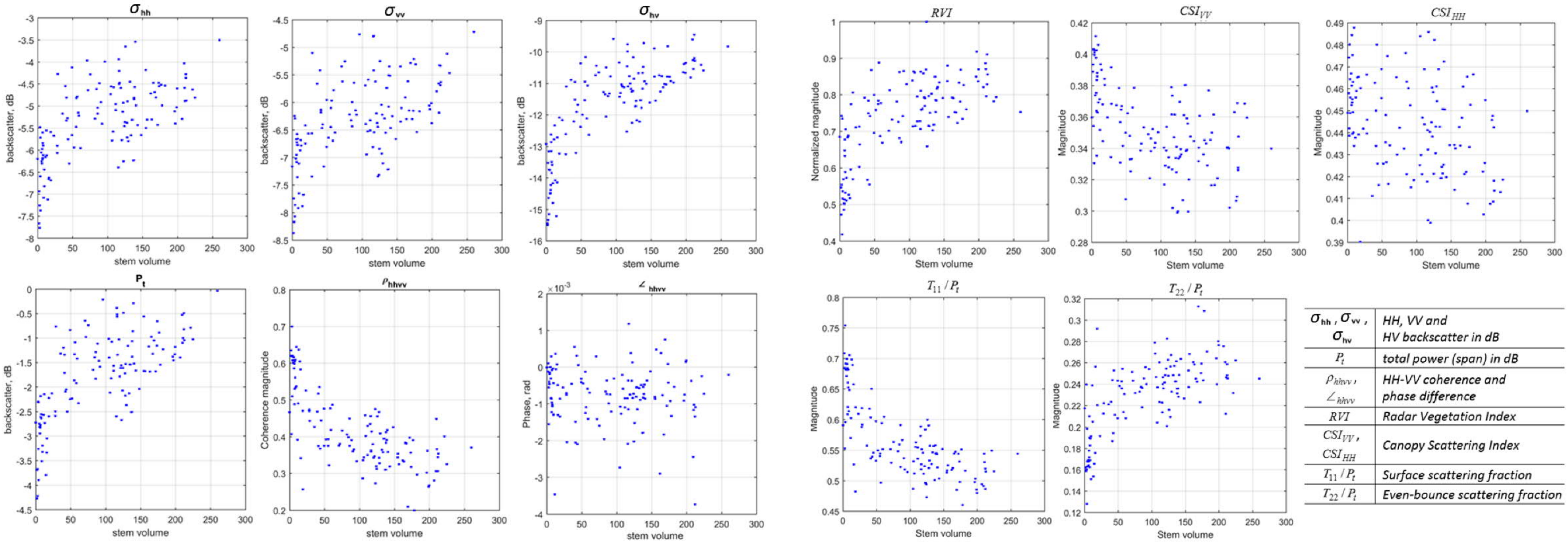

σ_{hh}, σ_{vv}, σ_{hv}	*HH, VV and HV backscatter in dB*
P_t	*total power (span) in dB*
ρ_{hhvv}, $\angle_{hhvv}$	*HH-VV coherence and phase difference*
RVI	*Radar Vegetation Index*
CSI_{VV}, CSI_{HH}	*Canopy Scattering Index*
T_{11}/P_t	*Surface scattering fraction*
T_{22}/P_t	*Even-bounce scattering fraction*

Antropov et al., Polarimetric ALOS PALSAR Time Series in Mapping Biomass of Boreal Forests. *Remote Sensing*. 2017; 9(10):999.

- InSAR to forest biomass relationship (hemiboreal forest at X-band)

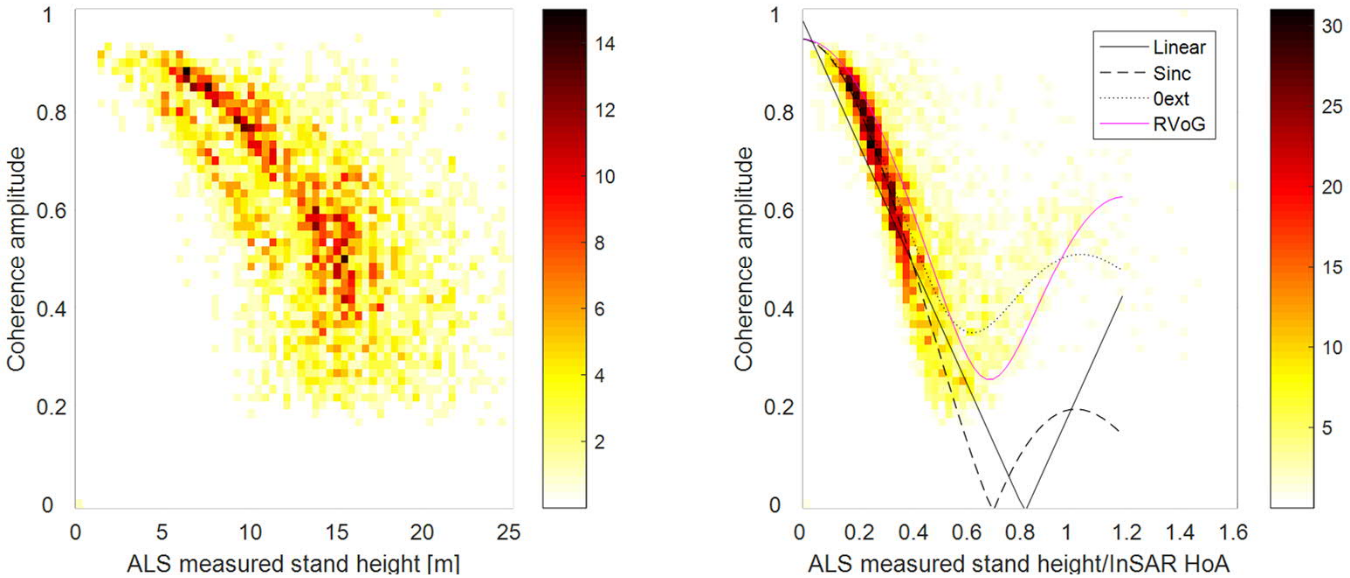

A. Olesk et al., Interferometric SAR Coherence Models for Characterization of Hemiboreal Forests Using TanDEM-X Data, Remote Sensing 8.9 (2016), p. 700.

Change detection (CD) approaches

- Simple considerations
  - bi-temporal CD approaches are preferred over monotemporal (single image classification into change/no-change classes)
  - Post-classification CD is generally suboptimal
  - Multitemporal CD approaches are preferred over all others
  - No need to use exclusively EO sensor data (DEMs, weather data)
- Feasibility of approaches depends:
  - Data type (e.g., SAR, InSAR, Pol-InSAR, TomoSAR)
  - Sensor wavelength
  - Acquisition geometry
  - Algorithmic approach and data continuity
  - Quality of reference dataset
  - Data costs and availability

Algorithmic approaches to change detection

Feature calculation (pixel- or stand-level)

- sequence of measurements as independent features
- various ratios, moments
- time signal based features (to account for temporal dynamics)

Change implemented as

- Statistical hypothesis testing (e.g. distance between pdfs).
  Can also deliver probabilistic information and change magnitude.
- Post-classification (post-retrieval) change detection.
  Often needs auxiliary data and exhibits lower accuracy, however explicit information on class transitions.
- Classifier in binary or multiclass classification using “image time series” or “change signal” . Statistical post-processing can be used to derive uncertainties.
- Deep learning classification or change-detection can be done.

Algorithmic approaches to change detection

Supervised approaches

- Random forests,
- SVMs,
- maximum likelihood
- kNN (ikNN)
- logistic regression

Non-supervised approaches

- K-means,
- iso-data,
- physics-based indicators, e.g., “radiometric contrast”

Weakly supervised approaches

Sampling and accuracy assessment

Sampling is critical is model training and accuracy assessment.

- Sampling design – non-stratified (simple) and stratified approaches
    - Random sampling
    - systematic sampling

Thematic accuracy assessment based on confusion matrix

Accuracy measures

- User’s and producer’s accuracies
- F-1 score
- Cohen’s kappa

Recent developments in forest change mapping

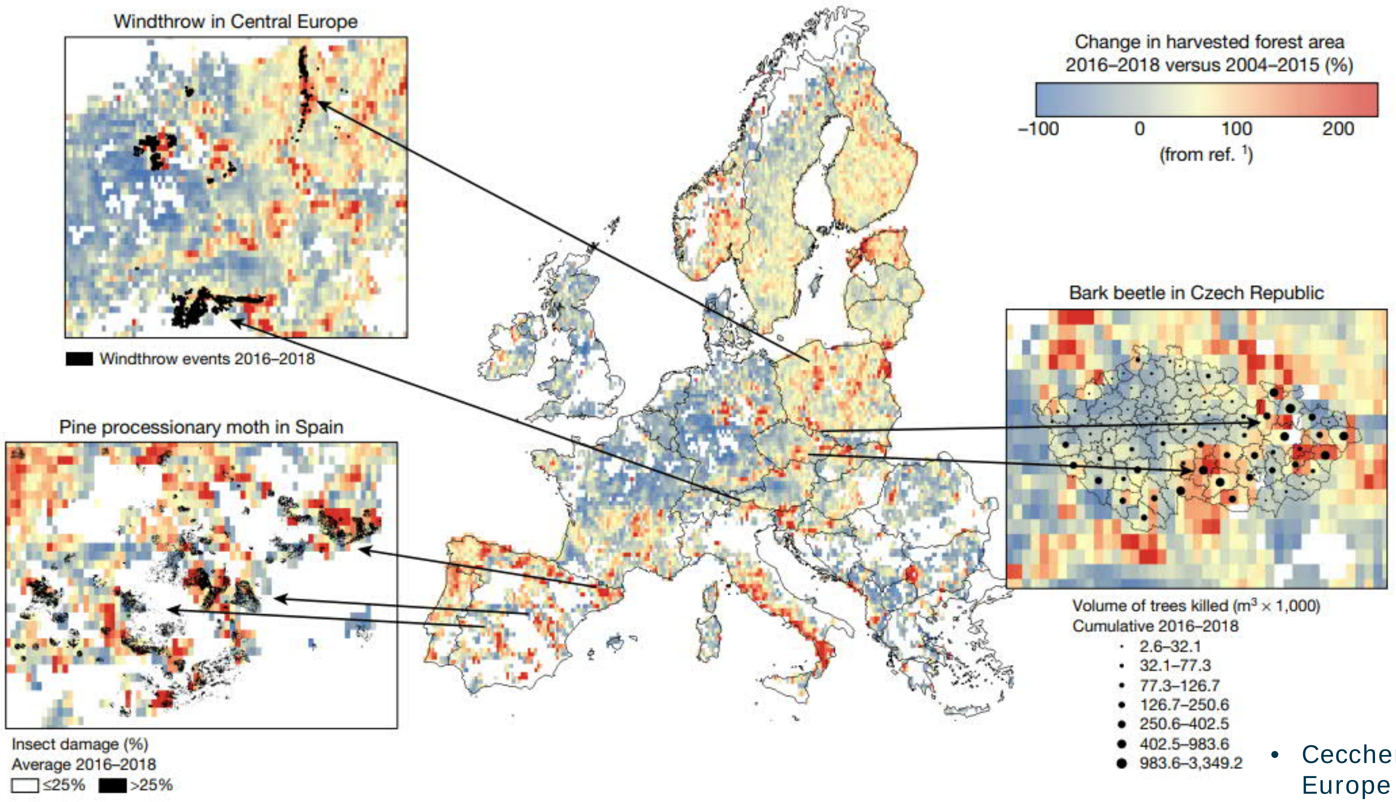

Areas identified as natural disturbances.

Forest mapping difficulties:

- Interpretation/attribution of change
- Possible over/underestimation of change based on EO data quality
- Heavy weight on EO value-added products
- Lack of reference data

Sample-based reference data provide the primary reliable source for area change estimation

- Ceccherini, G. et al. Abrupt increase in harvested forest area over Europe after 2015. Nature 583, 72–77 (2020).
- Palahí, M., Valbuena, R., Senf, C. *et al.* Concerns about reported harvests in European forests. *Nature* 592, E15–E17 (2021)

Data issues: mosaicking

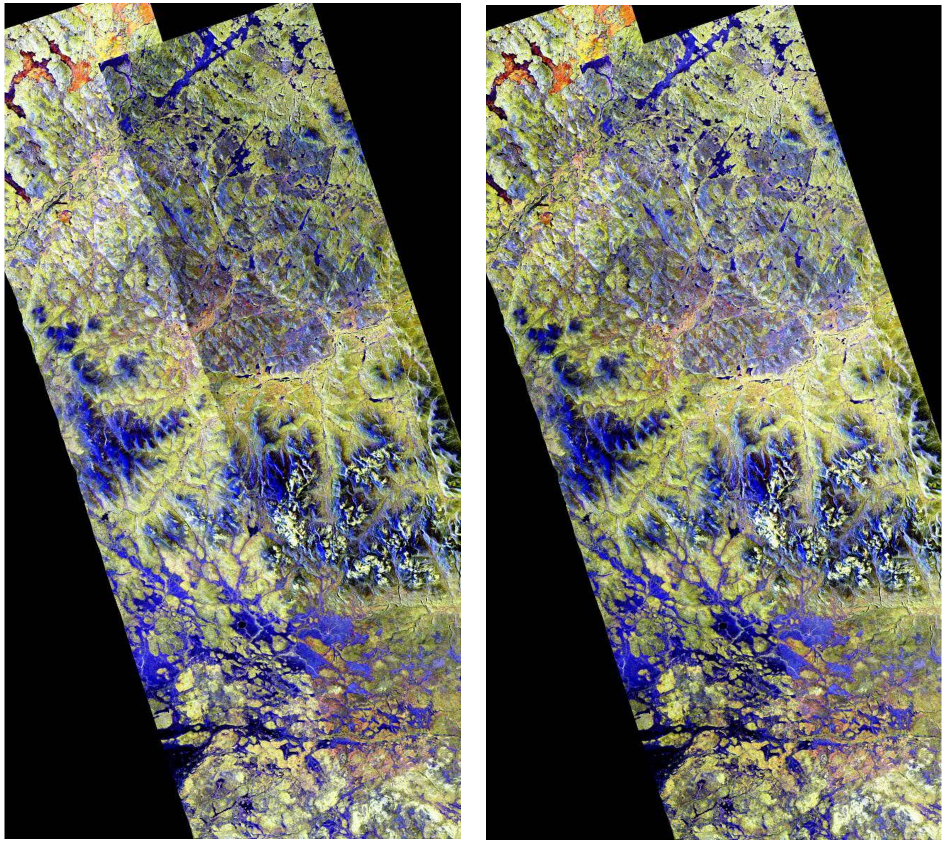

Antropov et al., PolSAR mosaic normalization for improved land cover mapping, IEEE GRSL, 2012, ©IEEE

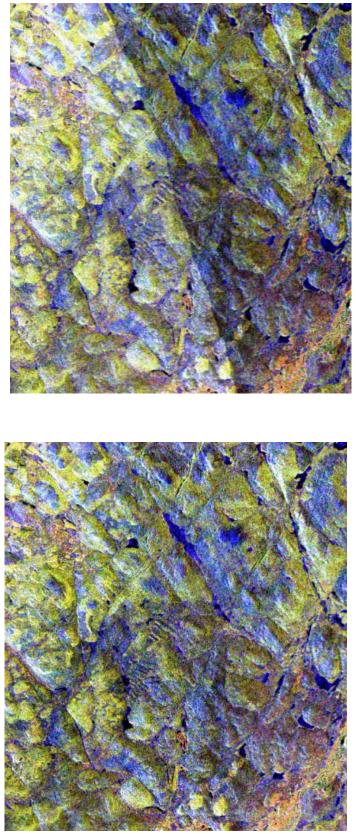

Rosenqvist et al., An overview of the JERS-1 SAR Global Boreal Forest Mapping (GBFM) project, IGARSS 2004, ©IEEE

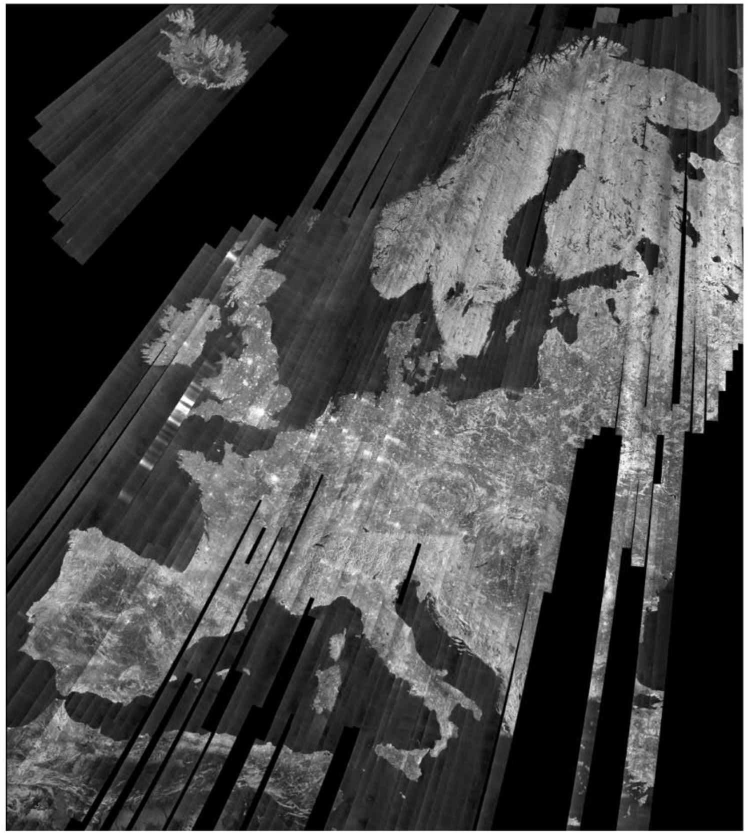

100 m JERS-1 SAR mosaic over Europe (1997/98). (incomplete draft). GBFM © JAXA/JRC/JPL

Data issues: seasonal variation

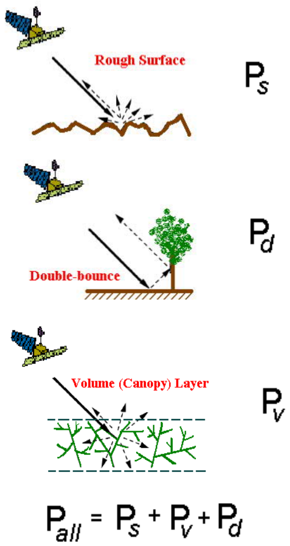

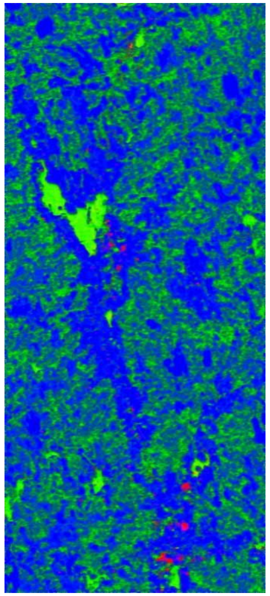

PolSAR RGB composite, Kuortane, Finland, November 2007

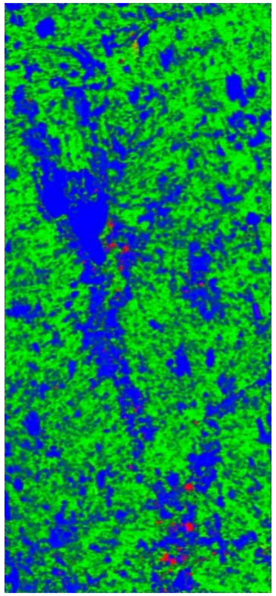

PolSAR RGB composite, Kuortane, Finland, May 2008

P_v

P_s

P_d

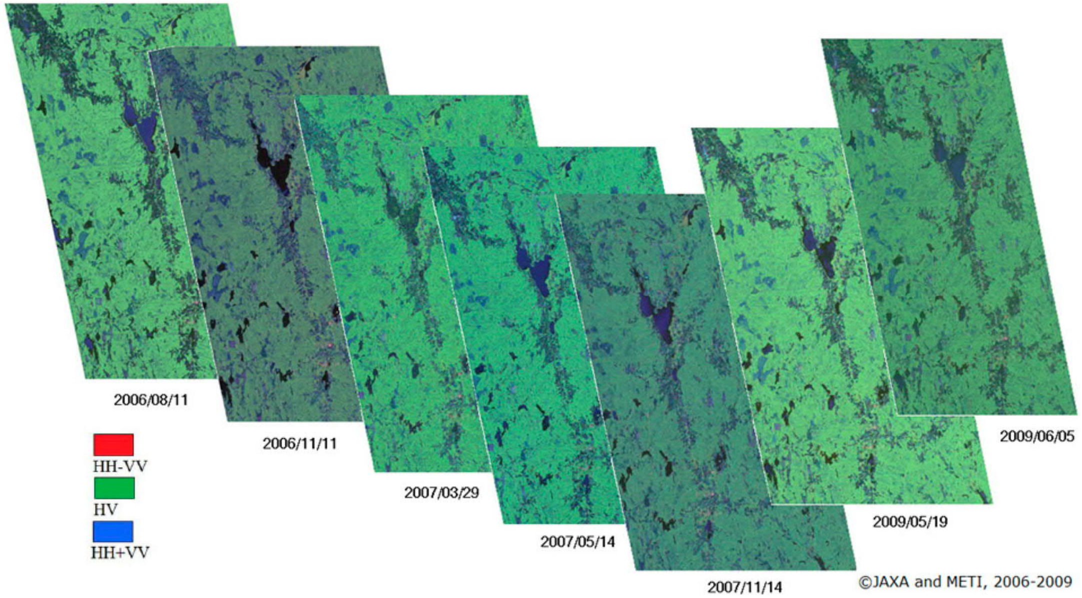

Antropov et al., Volume scattering modeling in PolSAR decompositions: Study of ALOS PALSAR over boreal forest, IEEE Trans. Geoscience Remote Sensing, 2011, ©IEEE

Antropov O, Rauste Y, Häme T, Praks J. Polarimetric ALOS PALSAR Time Series in Mapping Biomass of Boreal Forests. *Remote Sensing*. 2017; 9(10):999.

SAR data ”flattening”

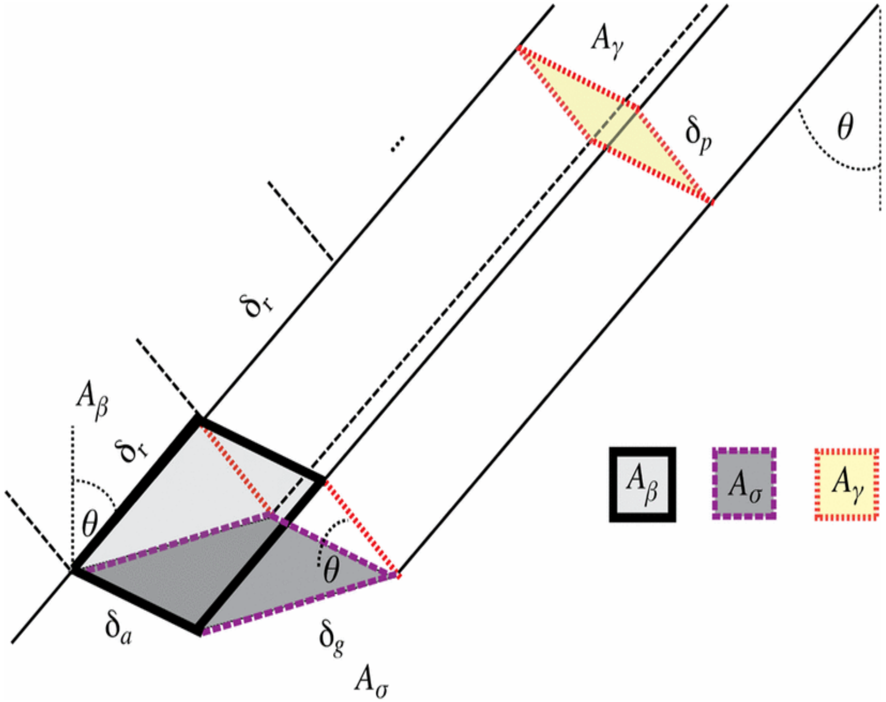

Normalization areas for SAR backscatter

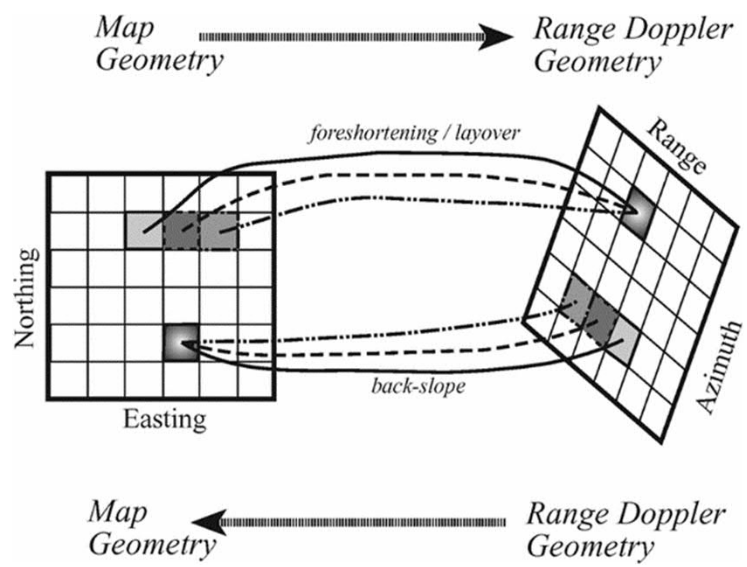

Topology of radar geometry

Small et al., Flattening gamma: Radiometric terrain correction for SAR imagery, IEEE Trans. Geoscience Remote Sensing, 2011, ©IEEE

SAR data ”flattening”

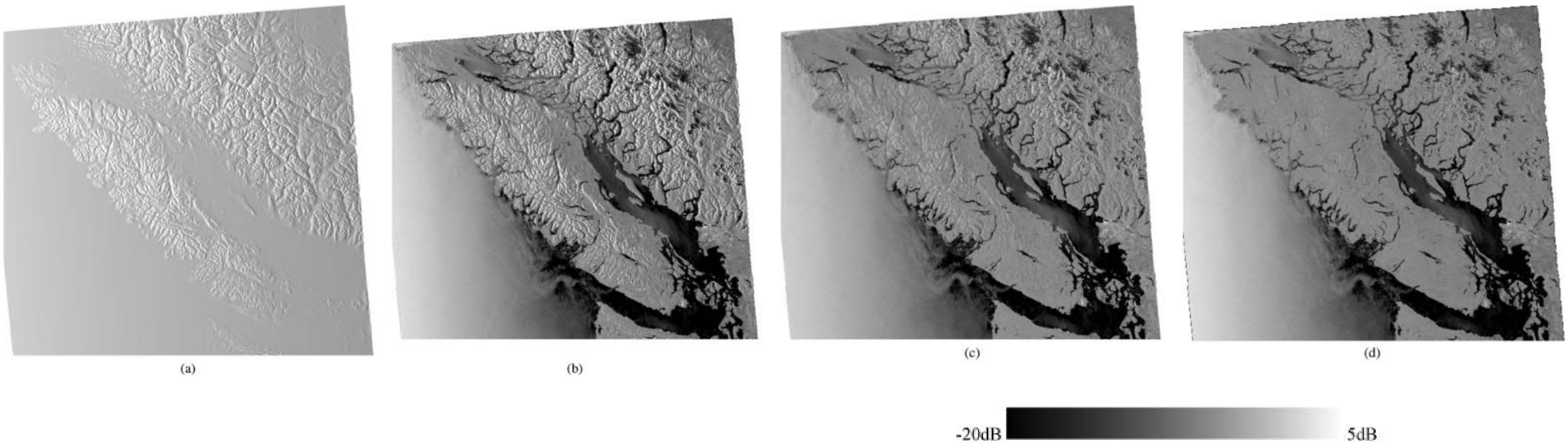

ENVISAT ASAR Wide Swath VV Image acquired on 2008.09.10 of Vancouver Island and southwestern British Columbia, Canada—SRTM3 DHM used for terrain-geocoding and radiometric corrections. (a) Local contributing area A_γ (image simulation), (b) γ_E^0 GTC, (c) σ_{NORLIM}^0 NORLIM, (d) γ_T^0 RTC.

Small et al., Flattening gamma: Radiometric terrain correction for SAR imagery, IEEE Trans. Geoscience Remote Sensing, 2011, ©IEEE

Demonstration Use-cases

Snow damage mapping: Introduction

Objective: to test the usability of Sentinel-1 observations in forest damage localization and severity assessment

- Test site, Kainuu, Finland
- In collaboration with Aalto university and Bitcomp
- Finnish Forest Centre data
- Background, serious snow damages late December 2107

Challenges:

The severity varies continuously

Imaging conditions, the temperature, snow, moisture, vary and affect backscattering

Aalto University

BITCOMP


Image: ©Sanna Härkönen

Tomppo, E.; Antropov, O.; Praks, J. Boreal Forest Snow Damage Mapping Using Multi-Temporal Sentinel-1 Data. *Remote Sens.* 2019, *11*, 384.

Snow damage mapping: Study area, SAR and reference data

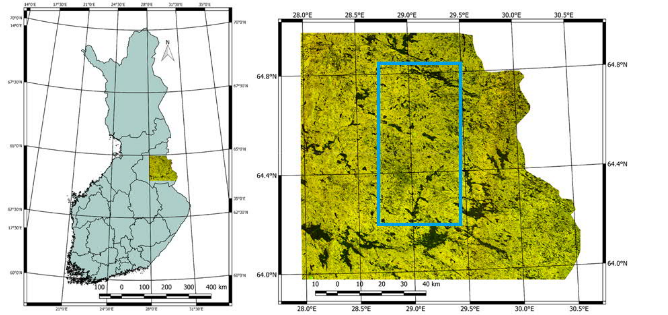

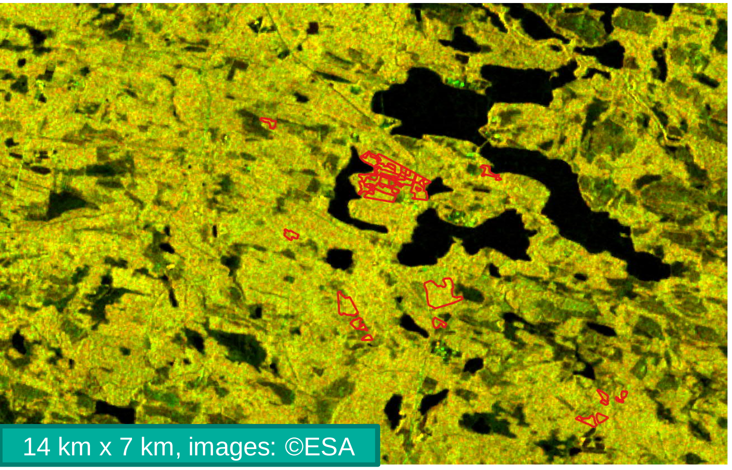

14 km x 7 km, images: ©ESA

Multitemporal composite of Sentinel-1 images (green-VH, red-VV). Red polygons denote sanitary cutting reports from Forest Centre (Metsäkeskus,2018).

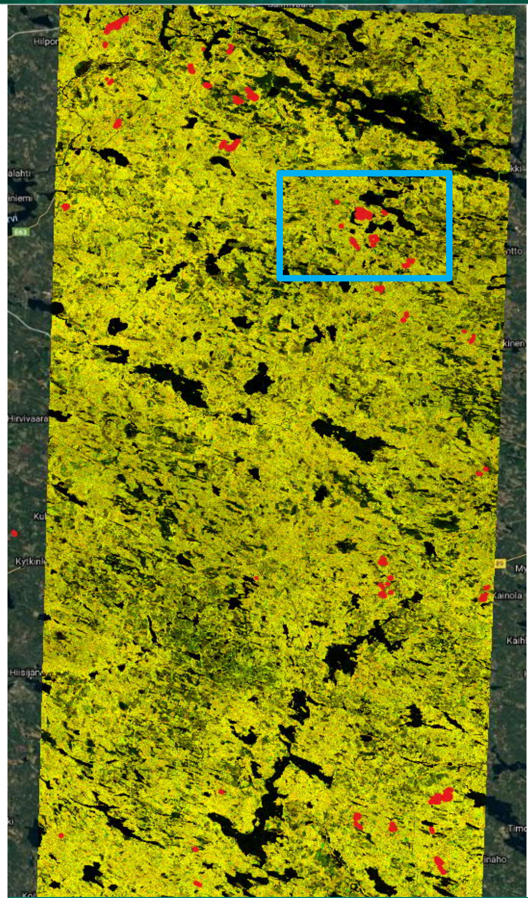

40 km x 80 km, images: ©ESA, ©Google Earth

List of Sentinel-1 scenes

Image	Date	Mode	Polarization
1	12 November 2017	IW	VV, VH
2	24 November 2017	IW	VV, VH
3	6 December 2017	IW	VV, VH
4	18 December 2017	IW	VV, VH
5	30 December 2017	IW	VV, VH
6	11 January 2018	IW	VV, VH
7	23 January 2018	IW	VV, VH
8	4 February 2018	IW	VV, VH
9	16 February 2018	IW	VV, VH
10	28 February 2018	IW	VV, VH
11	12 March 2018	IW	VV, VH
12	24 March 2018	IW	VV, VH

Reference data

Sanitary cutting reports were available from the Finnish Forest Centre (Metsäkeskus, 2018), along with MS-NFI data from Natural Resources Institute Finland (Luke, 2018 for sampling non-damaged stands.

Training and testing dataset: a sample of 929 damaged forest stands and a sample of intact forest stands.

Snow-damaged forest mapping: overall approach

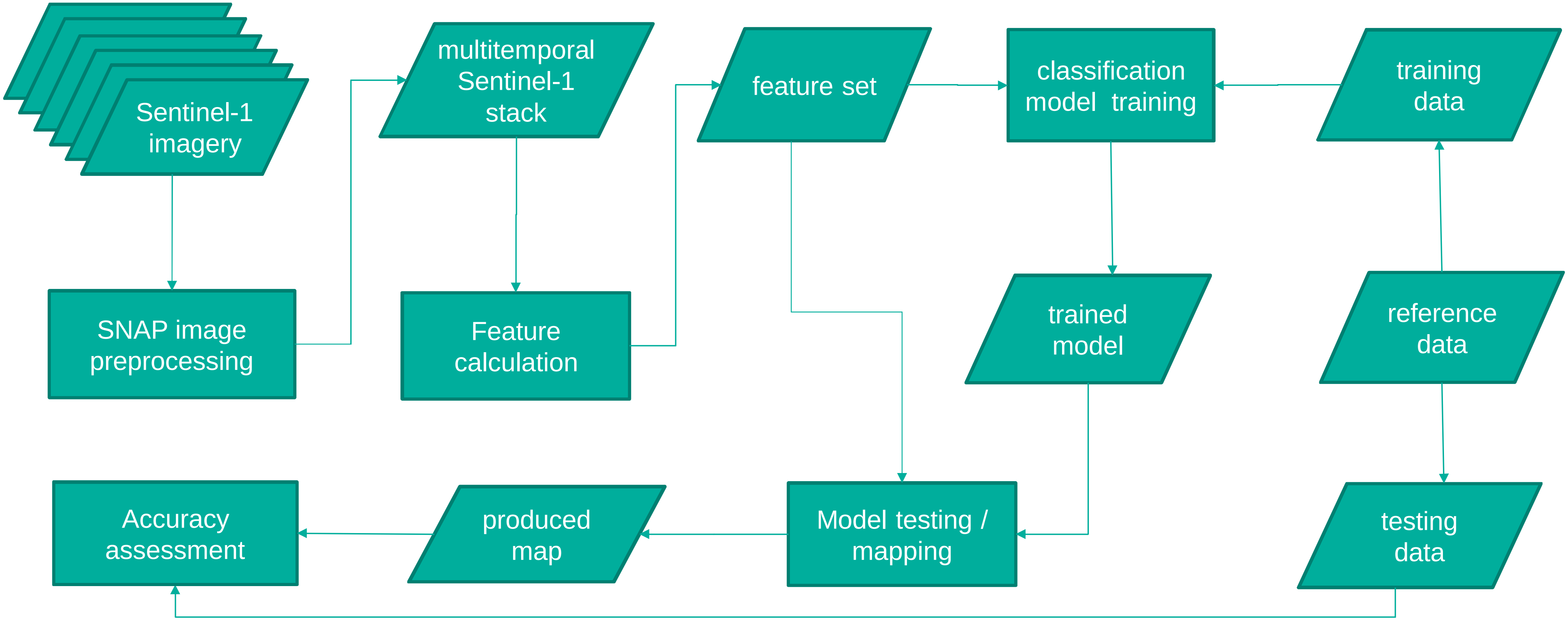

Snow-damaged forest mapping: SAR features and methods

Classification approaches:

- Logistic regression analysis for binary data (LR),
- an improved k-NN method (ik-NN) for categorical variables
- support vector machine (SVM)

From the pixel level intensities ($I_{s,i}^{k,pq}$), these backscatter features were calculated for each stand, s, for both polarizations pq and for each image, k, as follows:

(a) averages,

$$\overline{10\log_{10} I_s^{k,pq}} = 10\log_{10}\frac{\sum_{i=1}^{n_s} I_{s,i}^{k,pq}}{n_s}, k = 1,..,12,\ pq \in \{\mathrm{VV},\mathrm{VH}\},$$

where n_s is the number of the pixels in stand s,

(b) standard deviations

$$\sqrt{\sum_{i=1}^{n_s}(10\log_{10} I_{s,i}^{k,pq} - \overline{10\log_{10} I_s^{k,pq}})/(n_s-1)}, k = 1,..,12,\ pq \in \{\mathrm{VH},\mathrm{VV}\},$$

(c) ratios,

$$1/n_s \sum_{i=1}^{n_s} I_{s,i}^{k_1,pq} / I_{s,i}^{k_2,pq}, k_1 = 2,3,4 \text{ and } k_2 = 5,6,7,8,9.$$

Snow-damaged forest mapping: Results

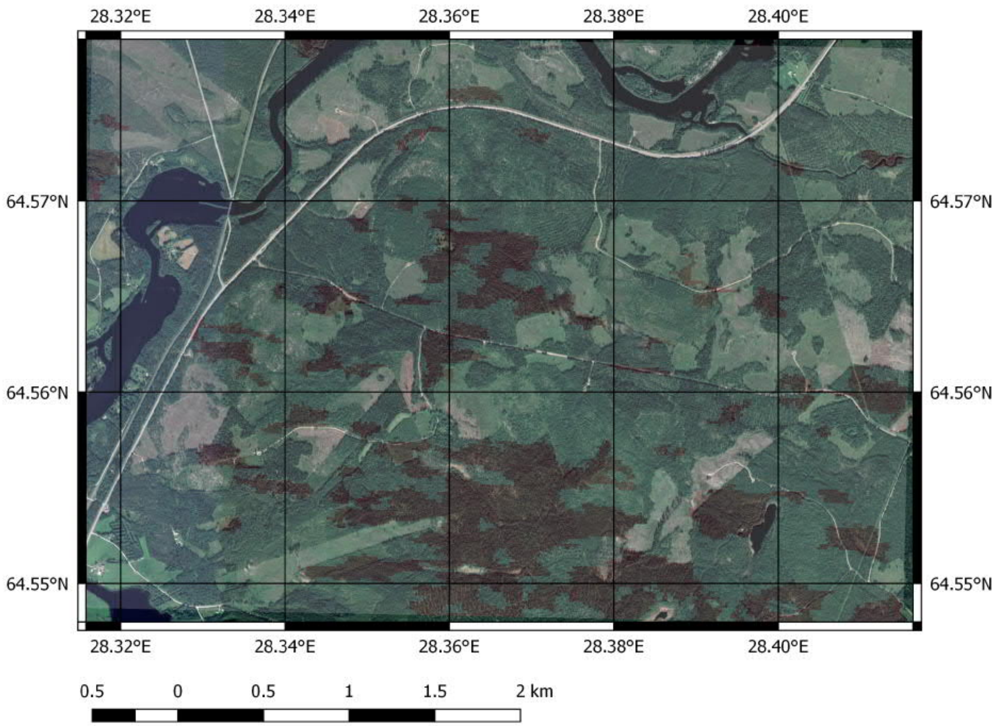

An example of snow-load damage map (brown) displayed on a Google Earth scene ©Google Earth. The area size is 4.8 km by 3.4 km.

Stand level accuracy metrics with separate validation data.

Method	Overall Accuracy	User Accuracy		Producer Accuracy	
		Damage	Non-Damage	Damage	Non-Damage
SVM	**0.91**	0.90	**0.91**	0.72	**0.97**
ik-NN	0.75	0.72	0.78	**0.80**	0.69
Logistic regression	0.71	0.69	0.73	0.76	0.67

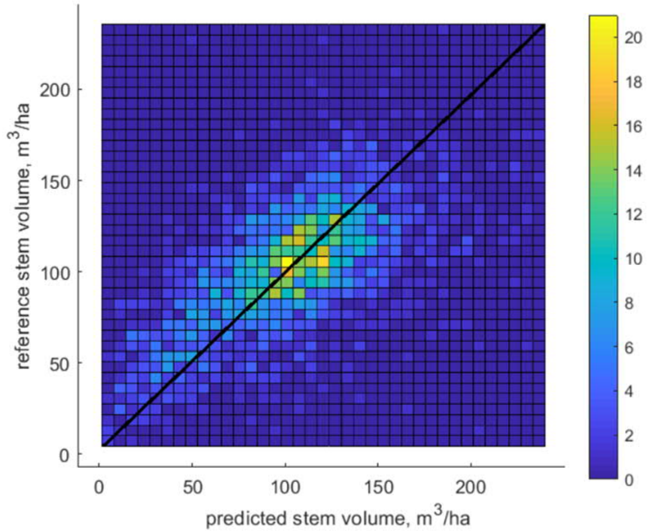

Tomppo, E.; Antropov, O.; Praks, J. Boreal Forest Snow Damage Mapping Using Multi-Temporal Sentinel-1 Data. *Remote Sens.* 2019, *11*, 384.

Snow damage mapping: Results

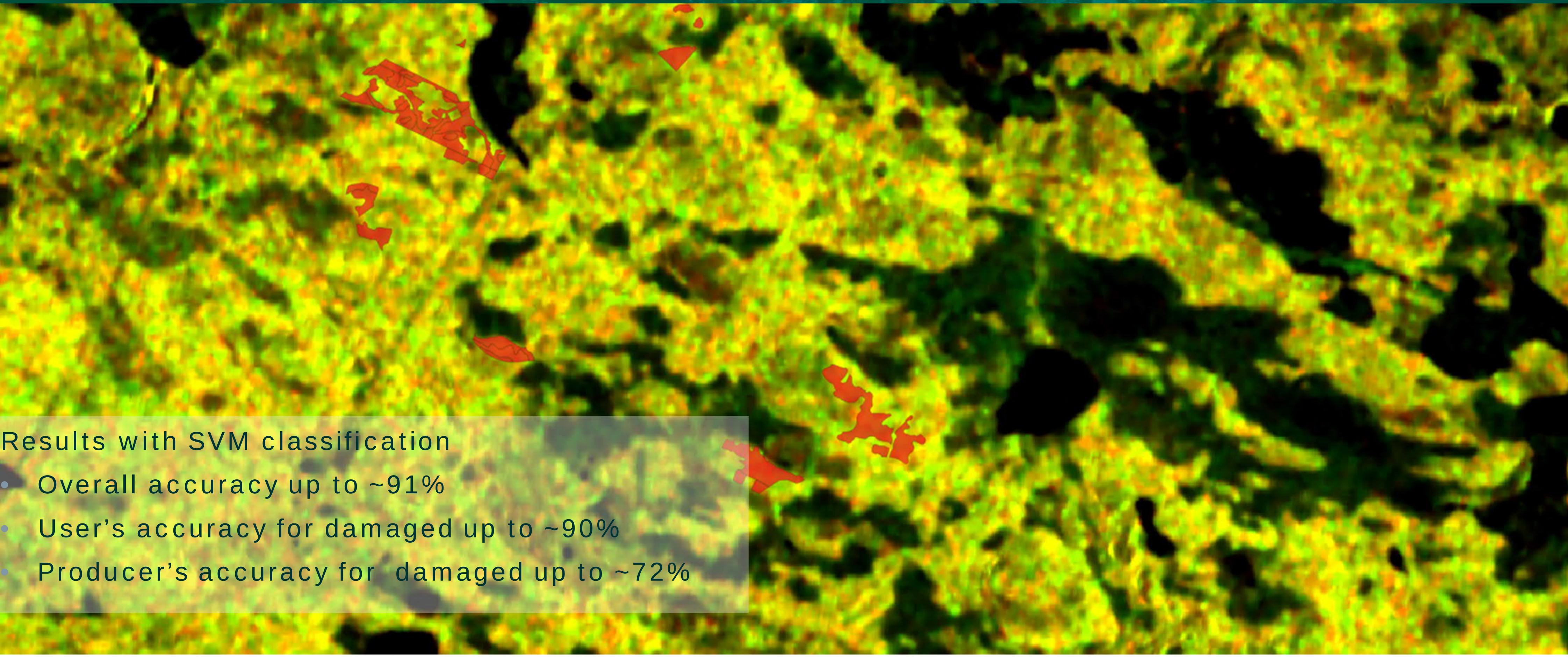

Results with SVM classification

- Overall accuracy up to ~91%
- User's accuracy for damaged up to ~90%
- Producer's accuracy for damaged up to ~72%

Windstorm damage

- Windstorms cause noticeable large area forest damages in Europe, including Scandinavia and Finland.
- In Finland, reported forest cuttings due to damage were over 30,000 ha in Northern Finland in 2014, and more than 6000 ha in Eastern Finland in July 2020.
- Rapid localization of the forest damages and removal of the fallen trees is the key for assessing the losses, as well as avoiding further damage, caused, e.g., by insects.

Tomppo et al., Detection of Forest Windstorm Damages with Multitemporal SAR Data—A Case Study: Finland. *Remote Sens.* 2021, *13*, 383.

Windstorm forest damage: Study area, SAR and reference data

...ral composite of Sentinel-1 images (green-VH,
...ed polygons denote sanitary cutting reports
...t Centre (Metsäkeskus,2018).

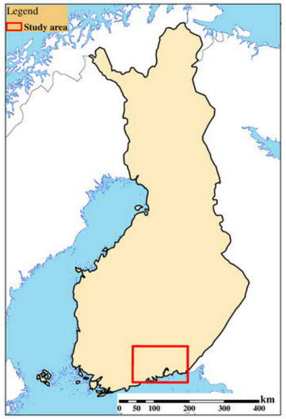

The location of the study area in Southern Finland.

The 27 Sentinel-1 data mosaics from 2017 used and their acquisition dates.

Mosaic	Date	Mosaic	Date	Mosaic	Date
1	4 January	10	14 July	19	20 August
2	16 January	11	15 July	20	1 September
3	28 January	12	21 July	21	7 September
4	9 February	13	26 July	22	12 September
5	21 February	14	2 August	23	13 September
6	2 July	15	7 August	24	18 September
7	3 July	16	8 August	25	19 September
8	8 July	17	14 August	26	24 September
9	9 July	18	19 August	27	25 September

Reference data

Data were selected in collaboration with Finnish Forest Centre (Metsäkeskus), along with MS-NFI data from Natural Resources Institute Finland (Luke) for sampling non-damaged stands.

Number of damaged stands was 313 (195 were severely damaged), non-damaged 664. The entire dataset was split into training (3/4) and validation dataset (1/4).

Separate analysis was done for the entire dataset and for stands with growing stock volume larger than 75 m^3/ha

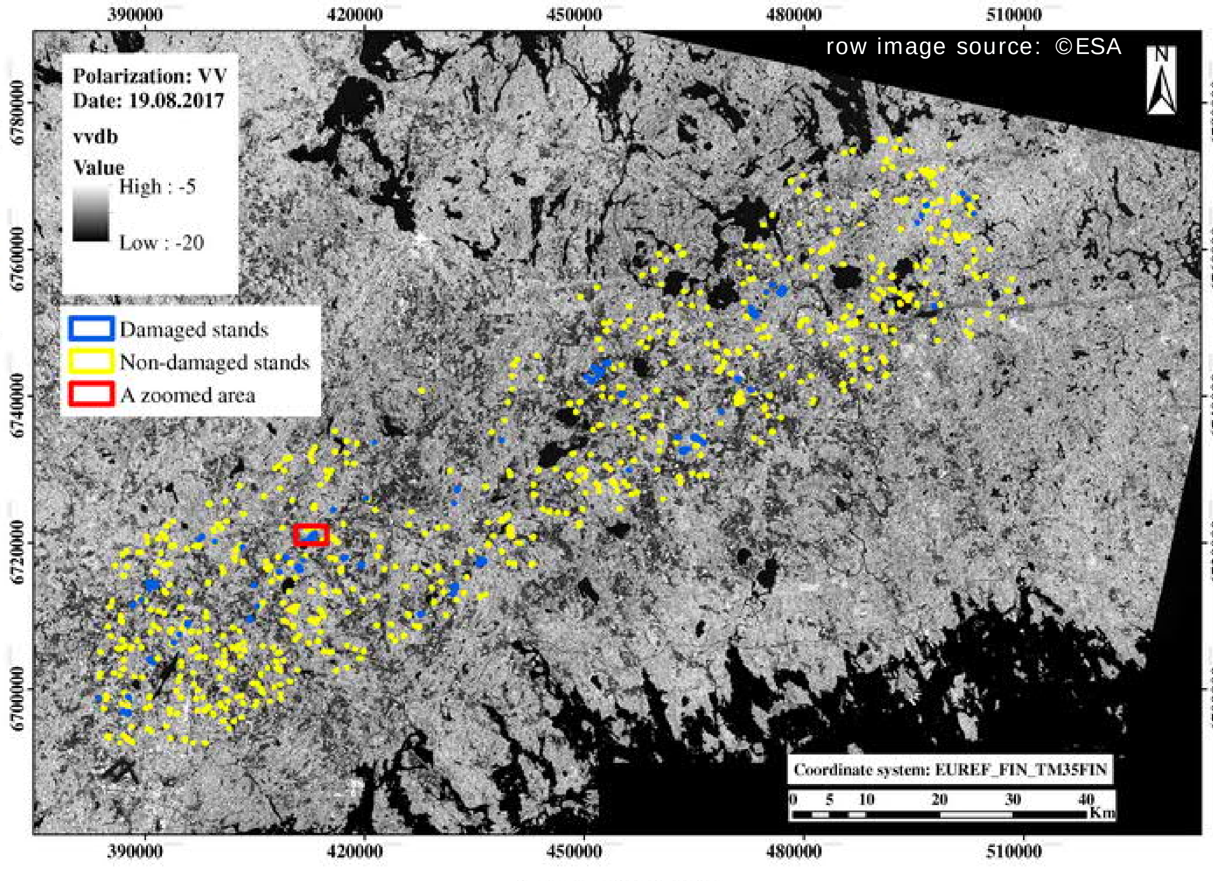

(a) VV 19.8.2017

Windstorm forest damage : additional data layer

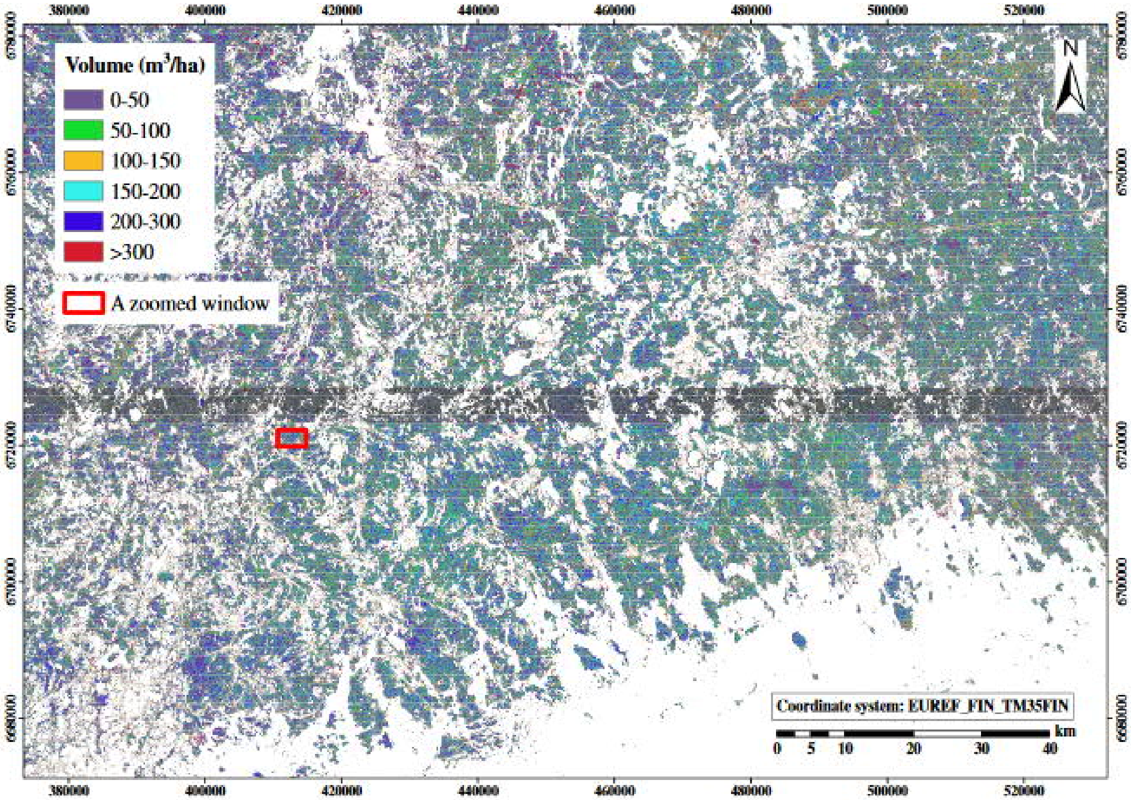

Volume of the growing stock on 31 July 2017 on the study area based on MS-NFI (EPS:3067).

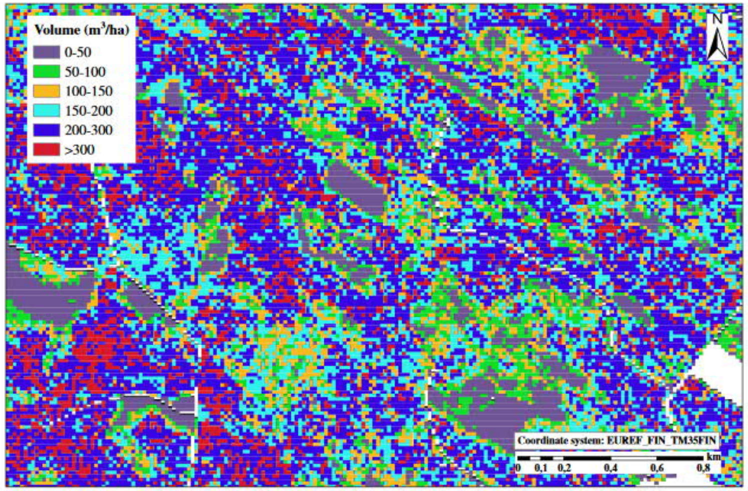

Additional explanatory variables in the models:

MS-NFI based:

- mean diameter of the trees,
- mean height of the trees,
- mean age of the trees
- basal area of trees
- growing stock volume by PFT.

DEM-based: average elevation, slope and aspect

Windstorm forest damage : classification methods

Classification approaches:

- the improved k-NN (ik-NN),
- Multinomial logistic regression (MLR)
- support vector machine classifier (SVM)

The observations units in the models were forest stand level

for each polarization p and for each image k:

(a) averages,

$$10\log_{10}\overline{I_s^{k,p}} = 10\log_{10}\frac{\sum_{i=1}^{n_s} I_{s,i}^{k,p}}{n_s}, k=1,\ldots,27, p\in\{\mathrm{VV},\mathrm{VH}\},$$

where n_s is the number of the pixels on stand s;

(b) standard deviations

$$\sqrt{\sum_{i=1}^{n_s}\left(I_{s,i}^{k,p}-\overline{I_s^{k,p}}\right)^2/(n_s-1)}, k=1,\ldots,27, p\in\{\mathrm{VH},\mathrm{VV}\};$$

(c) intensity-ratios

$$1/n_s\sum_{i=1}^{n_s} I_{s,i}^{k_1,p}/I_{s,i}^{k_2,p}, k_1=1\ldots,26 \text{ and } k_2=2,\ldots,27.$$

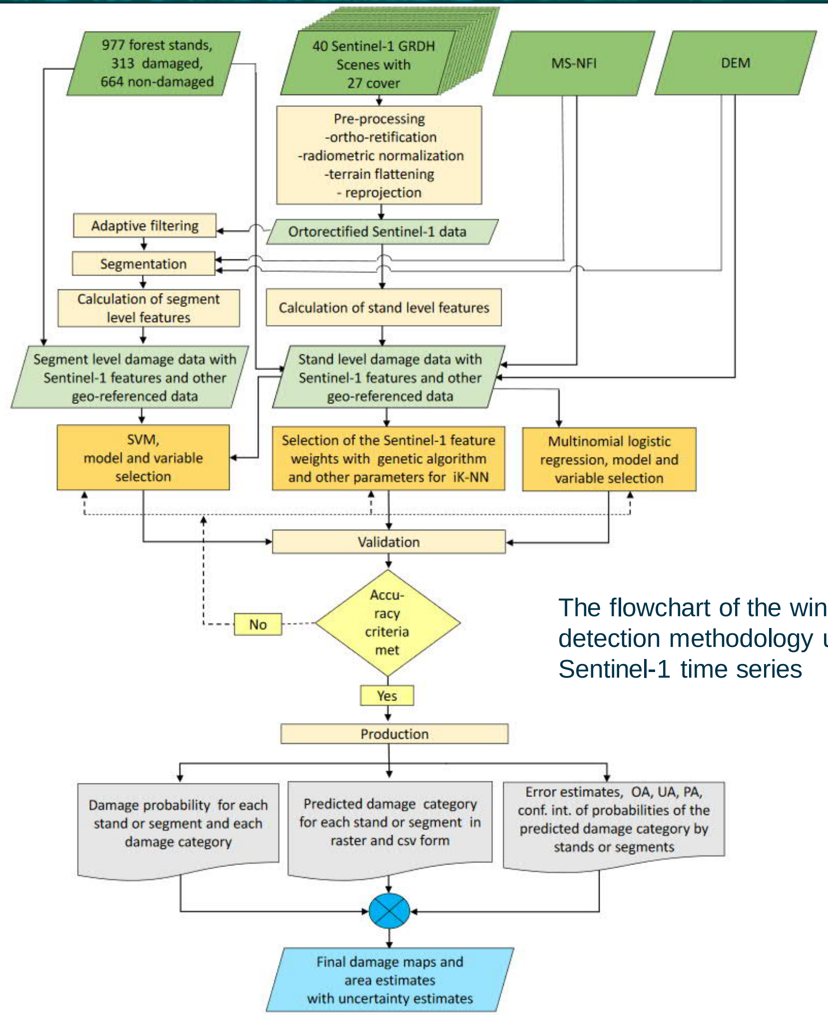

The flowchart of the windstorm detection methodology using Sentinel-1 time series

Windstorm forest damage: Results

The overall accuracy (OA), user's accuracy (UA) and producer's accuracy (PA) in the validation data using support vector machine (SVM), improved k-NN method (ik-NN) and multinomial logistic regression with four different Sentinel-1 datasets. The latest scene after the damage was from 20 August 2017, except for 27 scenes in which all Sentinel-1 scenes were used. Segmentation-based results are indicated with 'S'. A volume threshold of 75 m^3/ha was used for the data.

Method and the Number of the Scenes	OA	UA by Category			PA by Category		
		1 [1]	2 [2]	3 [3]	1 [1]	2 [2]	3 [3]
SVM 8 scenes	0.729	0.778	0.618	0.400	0.892	0.438	0.250
SVM 10 scenes	0.720	0.754	0.562	0.500	0.917	0.375	0.125
SVM 17 scenes	0.759	0.795	0.610	0.667	0.901	0.510	0.250
SVM 19 scenes	0.771	0.805	0.619	0.750	0.913	0.531	0.250
SVM 27 scenes	0.769	0.781	0.688	0.800	0.955	0.458	0.167
SVM 8 scenes, S	0.735	0.792	0.535	0.500	0.884	0.469	0.208
SVM 10 scenes, S	0.755	0.816	0.571	0.462	0.901	0.490	0.250
SVM 19 scenes, S	0.784	0.807	0.686	0.625	0.948	0.490	0.208
SVM 27 scenes, S	0.788	0.832	0.683	0.500	0.919	0.571	0.292
ik-NN 8 scenes	0.700	0.775	0.415	0.435	0.871	0.327	0.263
ik-NN 10 scenes	0.690	0.762	0.467	0.250	0.867	0.404	0.105
Ik-NN 17 scenes	0.703	0.781	0.432	0.434	0.867	0.365	0.263
ik-NN 19 scenes	0.630	0.747	0.286	0.133	0.814	0.308	0.053
MLR 8 scenes	0.703	0.742	0.435	0.583	0.917	0.208	0.292
MLR 10 scenes	0.712	0.763	0.464	0.533	0.904	0.271	0.333
MLR 17 scenes	0.686	0.771	0.407	0.348	0.879	0.229	0.333
MLR 19 scenes	0.657	0.794	0.326	0.296	0.808	0.286	0.333

[1] Damage, [2] Severe damage, [3] Slight damage.

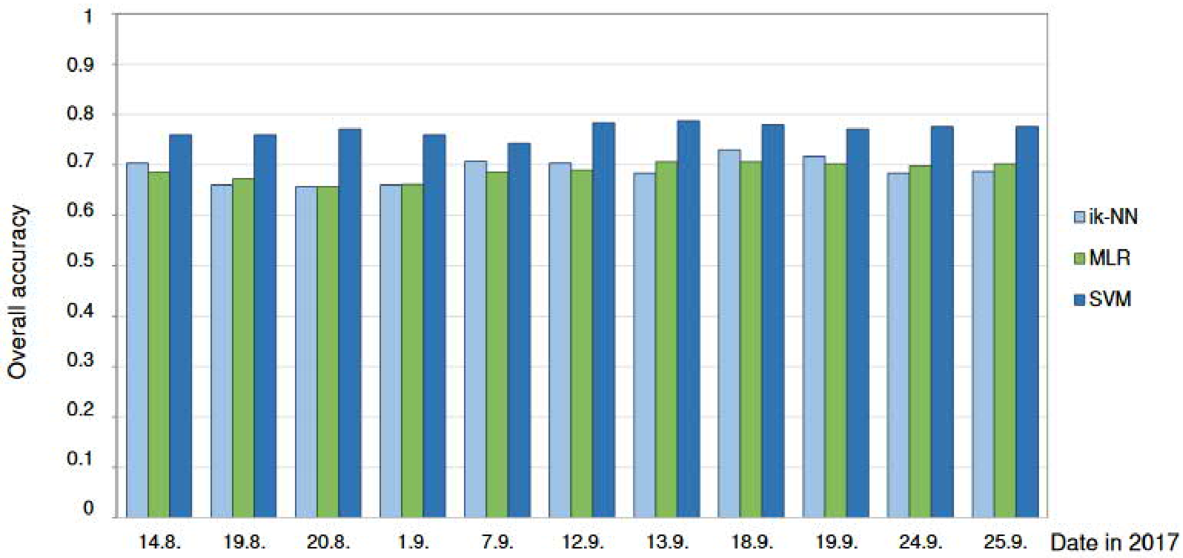

The overall accuracy with three different methods, ik-NN, MLR and SVM as a function of the acquisition date of the latest Sentinel-1 scene. The scenes were used until the date in the horizontal axis.

Windstorm forest damage: Results

- Support vector machine (SVM) gave the largest overall accuracies among the three methods tested, improved k-NN (ik-NN), multiple logistic regression (MLR) and SVM.
- The proportion of correctly classified stands (OA) in a separate validation data was 79%,and 75% if only one Sentinel-1 scene after the damage was used. The user’s accuracy(UA) for severe damages was 62%, and 75% for slight damages. The producer ’s accuracies (PAs) were somewhat lower.
- The accuracy of 75% was achieved using only one Sentinel-1scene after the damage, here two days after the damage, in addition to the data before the damage.
- Using segmentation-based calculation units only slightly increased the OA, implying that this approach may presume further work. Most likely, not only SAR data, but also inventory and other auxiliary data should be used in the segmentation methodology.
- The study indicates that the damages could be localized using only one Sentinel-1scene after the damage implying a time-lag of potential satellite SAR-based assessment method would be just a few days after the damage.

Windstorm forest damage : results and uncertainties

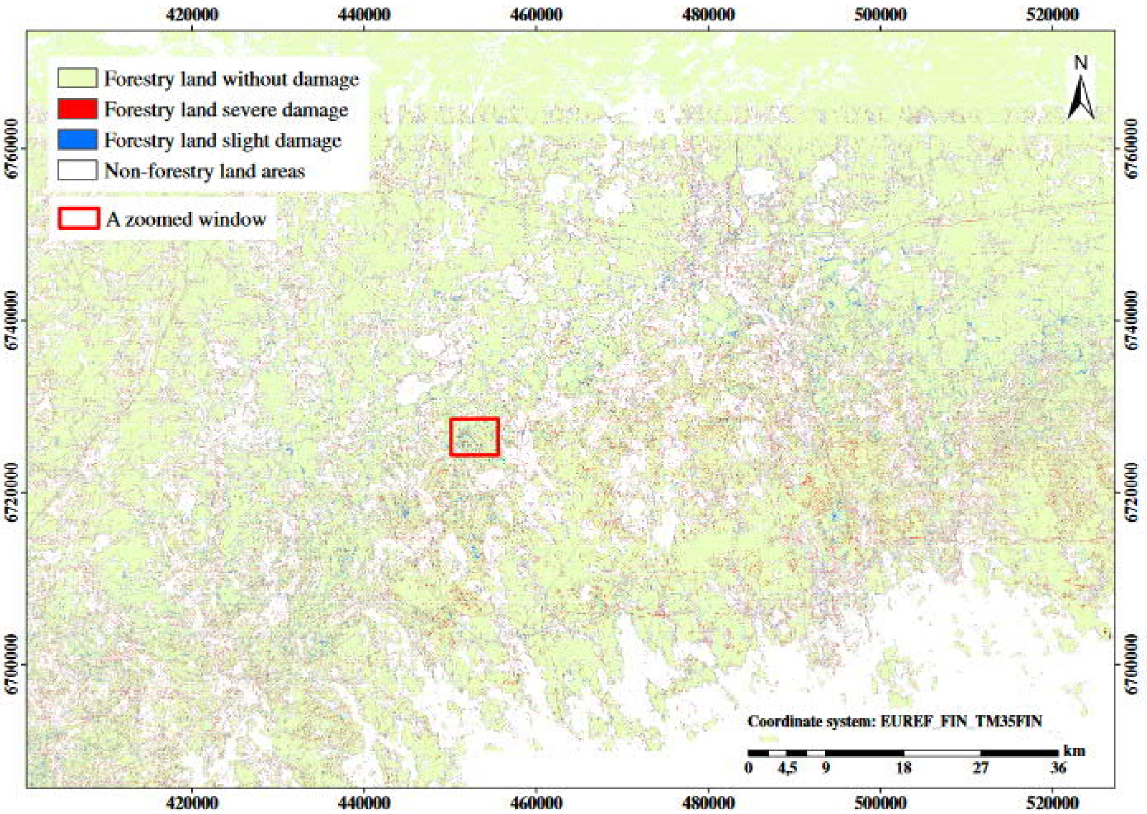

The predicted forest damages in the study area (EPGS:3067).

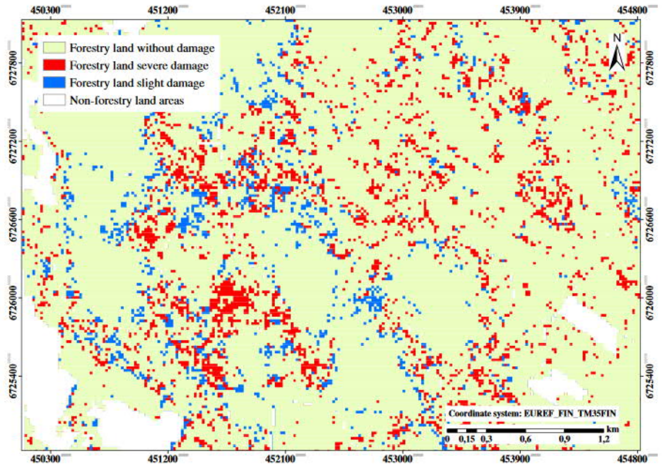

The predicted forest damages in a sub-area of the study area (EPGS:3067).

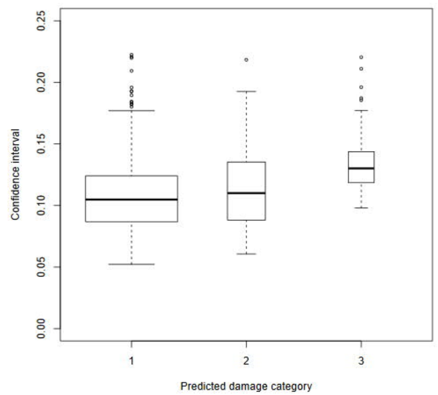

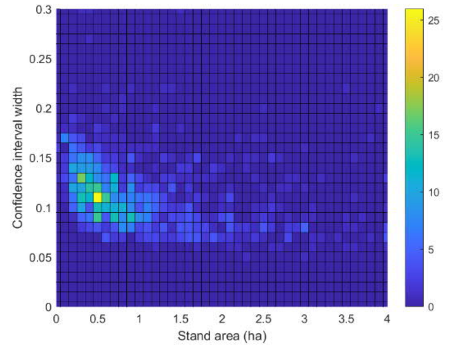

The width of the confidence interval of the probability of an individual prediction as a function of the area of the damaged stand.

VTT AutoChange approach

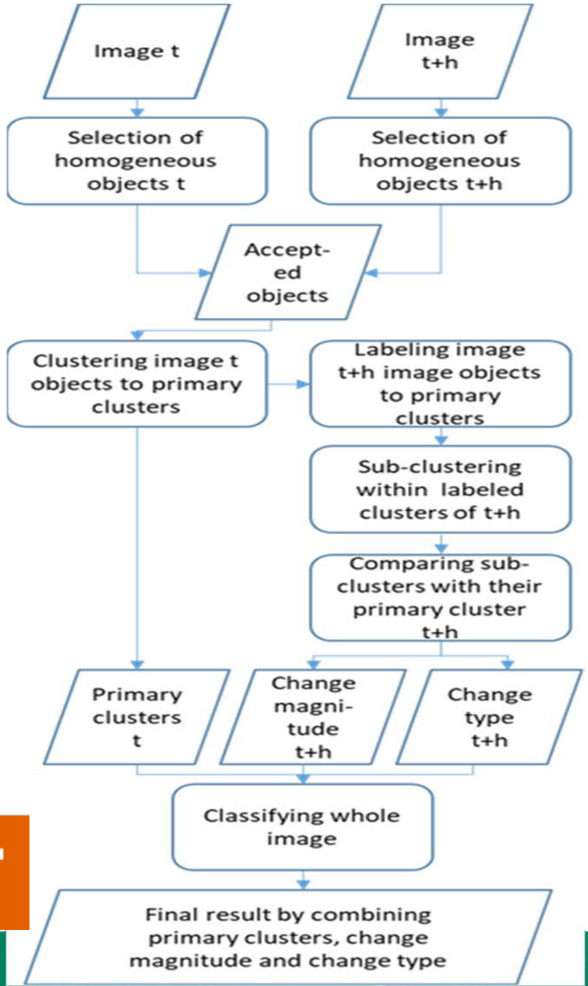

Image source: ©ESA

Figure 6. Output of S2-Autochange classification (3.6 x 3.6 km2)
(a) Sentinel-2A 2015,
(b) Sentinel-2A 2016,
(c) observations selected for clustering as white dots,
(d) primary clusters from pre-change image sorted by increasing red band reflectance,
(e) change type,
(f) change magnitude.

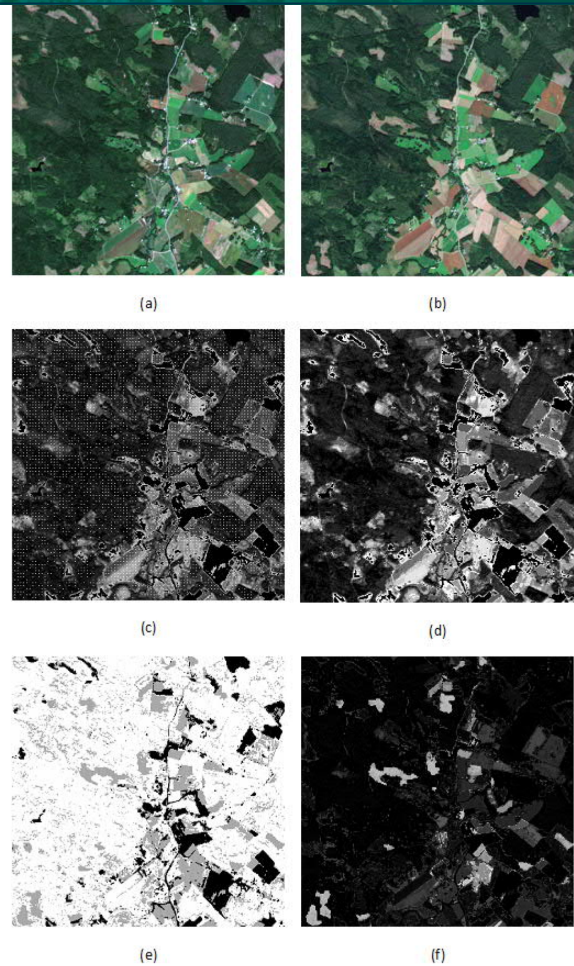

Häme et al. *Remote Sens.* 2020, *12*, 1751

AutoChange based monitoring of forest cover

AutoChange was tested:

- Forest cover change
- Forest harvesting
- Forest damages

Detected clear cuts in Ähtäri, Finland

Image source: ©ESA

Sentinel-2 August 2015

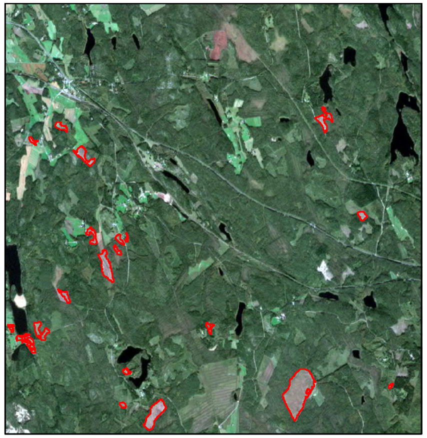

Sentinel-2 September 2016 and detected clear cuts 2015-2016

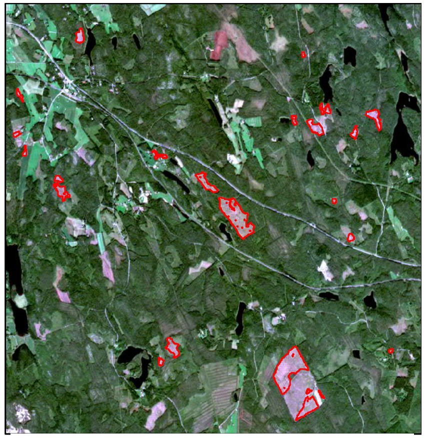

Sentinel-2 September 2017 and detected clear cuts 2016-2017

Forest cover change in Chiapas, Mexico

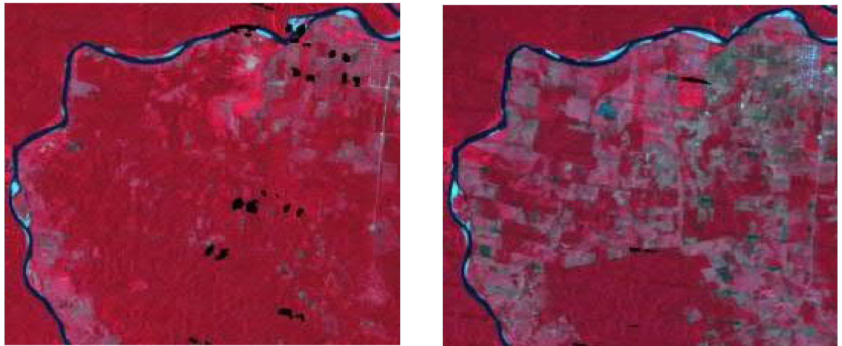

Image source: ©U.S. Geological Survey

Landsat false color composites

Produced forest cover maps

AutoChange based monitoring of forest cover

Detecting changes in forest during “Uuno” storm in June 2020 using AutoChange method and Sentinel-2 images in Kainuu in Finland

Size of the area is 1.6 km x 1.6 km

Sentinel-2 23.6.2020

Sentinel-2 29.6.2020

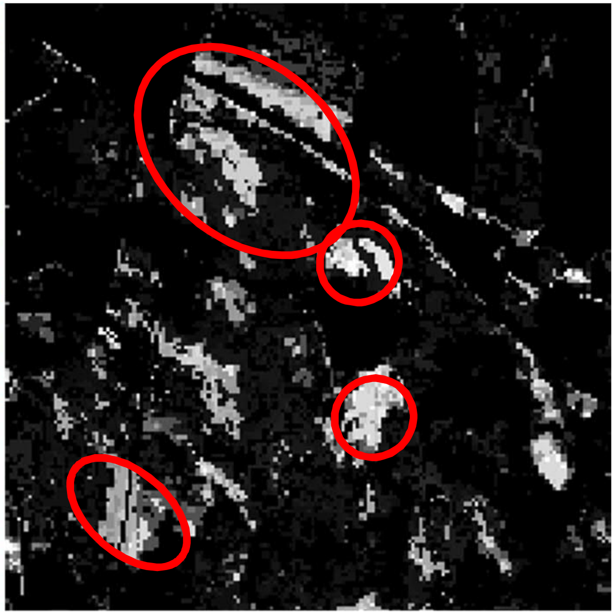

Change magnitude from AutoChange

L. Sirro, T. Häme, EU Forest Flux project, ongoing work

Conclusions

- Time-series are better than bi-temporal approaches or single-image interpretation
- Also auxiliary datasets, un addition to EO measurements, can be used
- Feature selection is important to identify most useful explanatory variables
- Sensor parameters and data continuity need to be carefully factored into analysis
- Reliable reference data and sampling design are critical
- Produced map (forest variable or change-map) is not very useful without uncertainty information